

Environment, Climate Change and Low Carbon Economy Programme

*'Environment Programme'*

*European Economic Area (EEA) Financial Mechanism 2014-2021*

A4 Report – Final products characterisation

28/07/2023

**37\_Call#2\_Circular Construction in Energy-Efficient Modular Buildings**

*Accordingly, with the Articles 25.2.j) and 29.4 of the 'Applicants Guide for Financing of Projects Supported by Environment, Climate Change and Low Carbon Economy Programme'*

[https://www.eeaqrants.gov.pt/media/2994/applicants-guide-for-financing-eea-grants\\_environment-projects\\_28112019.pdf](https://www.eeaqrants.gov.pt/media/2994/applicants-guide-for-financing-eea-grants_environment-projects_28112019.pdf)

## 1. Introduction

This report presents the actions developed during activity A4 – Final products characterisation, performed between September 2021 and July 2023. A4 was one of the core activities of the Circular2B project since it is related to the developed products and system.

This activity was divided into three actions carried out by UTAD, FEUP and Dreamdomus the partners:

- Hygrothermal characterisation of the core insulation material solutions;
- Hygrothermal characterisation of finishing render solutions;
- Hygrothermal characterisation of the SIP panel rendering system.

This task was developed by UTAD, FEUP and Dreamdomus, which gave valuable contributions regarding technological knowledge and market needs.

UTAD produced all the specimens (of the different formulations) required for the experimental campaign on some occasions with the collaboration of FEUP. FEUP was responsible for all the hygrothermal characterisation of the various solutions and for the mechanical resistance and optical performance of the rendering system. Dreamdomus was responsible for the adaption and optimisation of the production process of the panels, assembling and preparing all the panels

needed for the experimental characterisation. Also, Dreamdomus built the SIP panel prototype wall with 2x2m<sup>2</sup> and 15 cm thickness for thermal resistance determination at FEUP facilities.

Regarding the project indicators defined for A4, Circular2B contributed to incorporating recycled plastic, C&D waste (glass and ceramic) and recycled solid waste (fly ashes and wood waste) into the new SIP panel rendering system, as described in the Project Final Report. In summary, considering the construction of 12 modular houses per year with the new products, according to Dreamdomus data, the following annual consumption prediction amounts could be achieved:

- Recycled plastic: 26.8 tons;
- C&D waste (glass and ceramic): 0.2 tons;
- Recycled solid waste (fly ashes and wood waste): 509.6 tons.

## 2. Hygrothermal characterisation of the core insulation material solutions

### 2.1. Detailed characterisation of the most promising formulations

#### 2.1.1. Framework and experimental methodology

This action characterised the most promising formulations developed in Activity 3 and the selected formulations with nanoparticle incorporation for the core panel. The selected formulations presented a good compromise between the density and mechanical properties regarding the application purpose as a core insulation for SIP panels.

Table 1 presents the tests, the standard methods on which the tests were based and the specimens of the selected formulations, both with and without nanoparticles.

Table 1: Experimental tests and specimens of the five selected formulations

Test	Standard method	Specimen dimensions (mm)	Specimen quantity of each formulation
Thermal conductivity (dry state)	EN 12667 – Guarded hot plate method	300x300x30	2
Thermal conductivity/ Specific heat (dry state, 50% RH, 80% RH and saturated)	EN 1745 – Modified transient plane source method	100x100x30	3
Water content (50% RH, 80% RH and saturated)	ISO 12571	100x100x30	3
Porosimetry	ISO 15901	Small pieces	3
Dynamic modulus of elasticity/ Poisson's coefficient	EN 14146	100x100x100	3

One formulation with and another without nanoparticles will be selected and subjected to a complementary characterisation, as shown in Table 2.

Table 2: Selected formulations for the complementary characterisation

Test	Standard method	Specimen dimensions (mm)	Specimens quantity of each formulation
Water vapour permeability	ISO 12572	210x210x20	6
Capillary water absorption	EN 1015-18	160x40x40	3
Adhesive strength (testing of different adhesive products)	EN 1015-12	200x200x40	3

Also, the selected core insulation material was analysed in terms of the curing process – hot (drying in the oven) or ambient conditions- by a preliminary thermal conductivity and adhesion analysis.

To reach the dry state, the specimens were placed in an oven WTC Binder (see Figure 1-a). The 50% and 80% equilibrium was achieved using a climatic chamber with the required RH and 23° C (see Figure 1-b).



a)



b)

Figure 1: Conditioning equipment a) oven; b) climatic chamber.

a) Thermal conductivity, specific heat and water content

The thermal performance was first evaluated by measuring the thermal conductivity in the dry state through the Guarded Hot Plate method based on the European standard (EN 12667, 2001) using the Holometrix GHP-300 test equipment (see Figure 2). Two samples of each formulation were produced, as shown in Figure 3. For this test, it is required to ensure the flatness of the samples.



Figure 2: Holometrix GHP-300 – Guarded Hot Plate equipment.



Figure 3: Example of the specimens for thermal conductivity measurement using the Guarded Hot Plate Method.

The second available method – modified transient plane source – allowed the thermal conductivity and specific heat measurement at different conditions: dry state, 50% of relative humidity (RH)), 80 % RH and saturated. The equipment was the ISOMET 2114 model with a surface probe, as shown in Figure 4.



Figure 4: ISOMET 2114 – modified transient plane source equipment

Three specimens of each formulation were prepared by cutting the samples with the required dimensions (see Figure 5).

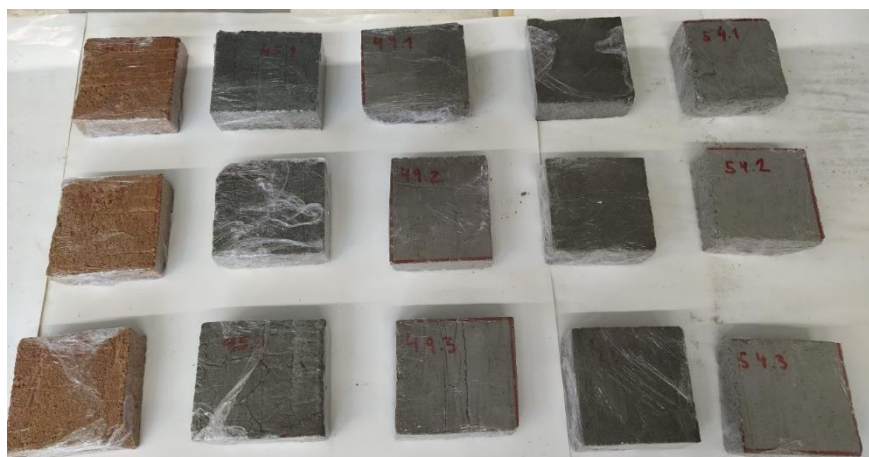


Figure 5: Example of the specimens for thermal conductivity measurement using the modified transient plane source method.

The determination of the water content was performed in parallel with the thermal conductivity after conditioning the samples at the required conditions (50% RH, 80 % RH and saturated) by weighing each specimen with a scale (see Figure 6), determining the mass at each condition comparing to the dry state mass.



Figure 6: Weighing samples for water content determination.

#### b) Microstructural analysis

The Mercury Intrusion Porosimetry (MIP) and helium pycnometer (HP) methods characterised the pore structure. Both methods assessed the pore size distribution and matrix properties using Quantachrome Poremaster equipment. The specimens consisted of small pieces of other specimens, which were then installed in a glass. The air was then removed, using a vacuum pump, before the mercury was forced inside, using both low (0.2 to 80 psia) and high (20.154 to 57785.242 psia) pressures, capable of mapping a pore size range between 10.584799 and 0.003692  $\mu\text{m}$ .

The bulk density and open porosity tests were performed by hydrostatic weighing according to the test report FE Pa 44 "Determination of open porosity and bulk and real densities" (LNEC 2015a). Three cubic specimens (measuring 40 mm per side) of each material (thermal render and finishing render) were prepared and conditioned. The test begins by placing the specimens in a desiccator for 24 hours in vacuum conditions. After this procedure, the samples were immersed for another 24 hours. The hydrostatic and immersed weights were then registered

#### c) Dynamic modulus of elasticity and Poisson's coefficient

A non-destructive test can determine the dynamic elastic modulus, measuring the fundamental resonance frequency, carried out according to the norm EN 14146 – "Natural stone test methods.



Determination of the dynamic elastic modulus of elasticity. These tests were performed in UTAD facilities.

d) Water vapour permeability

The water vapour permeability test was based on ISO 12572. Six specimens of each material of 210×210×20 mm were tested under two different ranges of relative humidity differences across the sample: wet cup and dry cup, in a climatic chamber. The climatic chamber presented controlled conditions:  $23 \pm 0.3^\circ\text{C}$  and  $50\% \pm 3\%$  relative humidity. The effective relative humidity in the cup test was obtained by using a  $\text{CaCl}_2$  compound ( $\text{RH} = 0\%$  for the dry-cup test) and a  $\text{KNO}_3$  solution compound ( $\text{RH} = 94\% \pm 0.6\%$  for the wet-cup test). The two test conditions – dry and wet cup – allow the evaluation of the water vapour permeability as a function of the relative humidity

Before testing, all the specimens are preconditioned in the climatic chamber at  $23^\circ\text{C}$  and 50% relative humidity. After stabilisation, the specimens are placed in metallic test cups, with the referred conditions being all sides sealed with paraffin wax, as shown in Figure 7.



Figure 7: Metallic cup and specimen sealed with paraffin.

e) Capillary water absorption

The capillary water absorption test allows the determination of the water absorption coefficient based on the European standard EN 1015-18. However, to calculate the coefficient of water absorption by capillarity ( $A_w$ ), which is used as an input parameter for hygrothermal simulation,

the test was adapted to measure various time intervals as indicated in ISO 15148 standard. Three specimens of each material of 160×40×40 mm were prepared, broken into two halves and then the four side faces sealed (see Figure 8).



Figure 8: a) Cutting the specimens into two halves; b) Sealing the sides with epoxy resin.

Before the test, the specimens are conditioned at room conditions (temperature and relative humidity) until a constant mass is reached. The test consists of measuring the specimens' mass precisely 10 minutes after they have been placed in water. This process is repeated at 90 minutes. According to ISO 15148 standard, water absorption by partial immersion is determined by measuring the mass difference of the analysed specimen, which is absorbed through the lower face in contact with water for at least 24 hours.

The specimens were placed inside a container with water on supports (see Figure 9), as should be done according to EN 1015-18, and then measured at the following time intervals: 5, 10, 20 minutes, 1, 1.5, 2, 4, 6, 8 hours, and finally, 24 hours.



Figure 9: Container for the capillary water absorption test.



f) Adhesive strength

The adhesive strength test is performed based on the EN 1015-12. According to EN 1015-12, the adhesive strength is determined as the maximum tensile stress applied by a direct load perpendicular to the surface of the rendering mortar on a substrate and is obtained by the quotient between the failure load in [N] and the test area, in [mm<sup>2</sup>]. Several specimens were produced (see Figure 10) to test the adherence of the core material to the OSB board, using different adhesive products (see Figure 11):

- Curing directly on the OSB board (Figure 11-a);
- Curing directly on the OSB board painted with a general primer (Figure 11-b);
- Core glued to the OSB board with polyurethane glue (Figure 11-c);
- Core glued to the OSB board with an adhesive mortar (Figure 11-d).

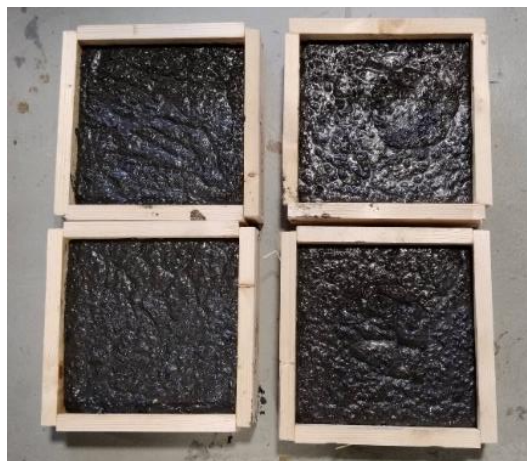


Figure 10: Production of specimens for the adhesive strength determination

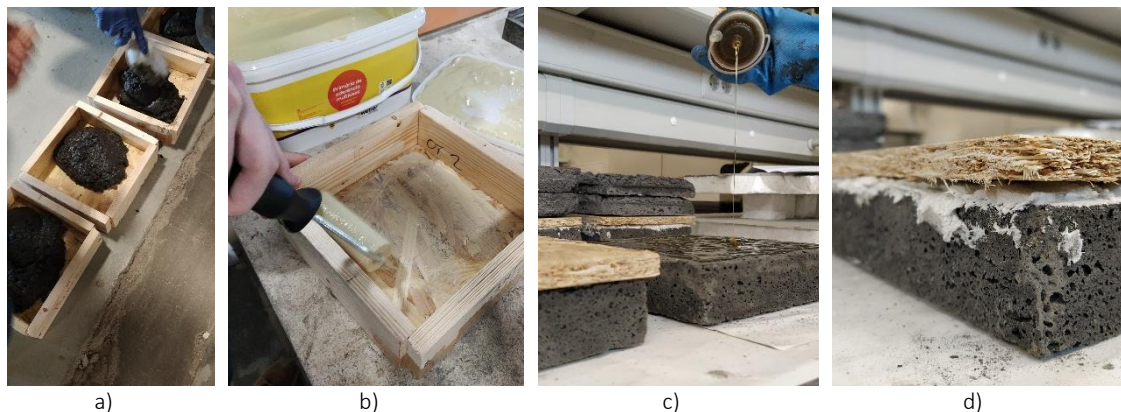


Figure 11: Different methods for adhering the core to the OSB board.

The test was performed using a testing machine – Proceq DY-216 (see Figure 12-a) – to apply the tensile load by means of a square pull-head (50x50 mm) glued to the test area (with epoxy resin) (see Figure 12-b). Despite EN 1015-12 indicating circular pull-heads, the test was performed using square pull-heads due to the great disturbance of the core drilling machine and the lower strength of the thermal mortars.

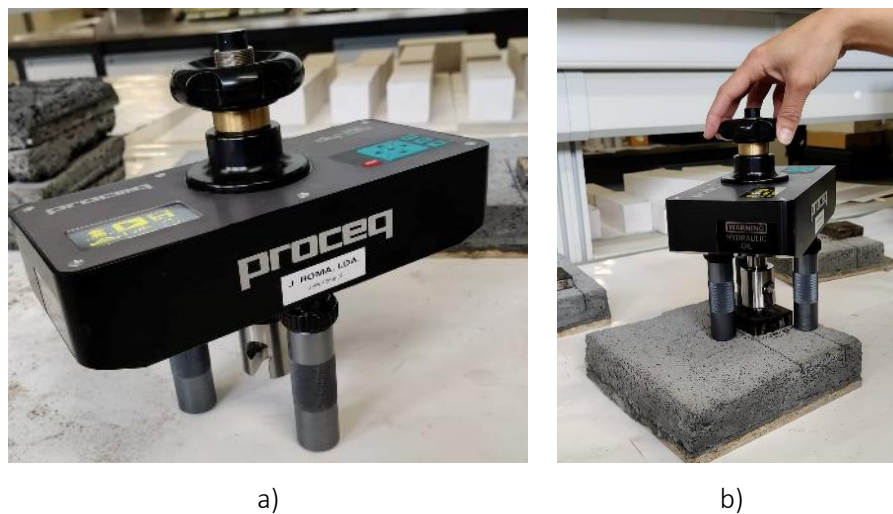


Figure 12: Adhesive strength test a) Pull-off equipment; b) Test set-up.

### 2.1.2. Formulations without nanoparticles

Table 3 shows the constitution of the five selected formulations.

Table 3: Selected formulations for the hygrothermal characterisation

Formulation	Marble	Granite	Fly Ash	Slag	Ceramic	Glass	PU	Timber	Powdered Aluminum	S/L	H/S
42	-	-	-	-	77%	17%	3%	3%	0.1%	0.55	0.80
45	-	45%	45%	-	-	-	5%	5%	0.1%	0.60	0.50
47	-	-	90%	-	-	-	5%	5%	0.1%	0.60	0.30
49	24%	-	24%	46%	-	-	3%	3%	-	1.00	0.50
54	45%	-	45%	-	-	-	5%	5%	0.1%	0.80	0.50

### a) Thermal conductivity - Guarded Hot Plate Method

Table 4 shows the results obtained with the Guarded Hot Plate Method.

Table 4: Results of the Guarded Hot Plate Method

Formulation	Average temperature (°C)	$\lambda$ (W/m°C)	Classification EN 998-1
42	10.17	0.113	T2
45	-	-	-
47	9.85	0.103	T2
49	9.87	0.119	T2
54	9.79	0.089	T1

Formulation 45, after being conditioned in the oven, became curved, which made it impossible to measure its thermal conductivity using the hot plate method. The specimens for this test need a smooth and flat surface to ensure the contact interface with the equipment remains intact.

Formulation 49, which consists of 24% marble, 24% fly ash, 46% slag, 3% polyurethane, and 3% wood, presents the highest thermal conductivity value. On the other hand, the material with the lowest thermal conductivity is 54, comprising 45% marble, 45% fly ash, 5% polyurethane, and 5% wood. One of the significant differences between the two formulations is the presence of slag in 49. Formulations 42, 47 and 49 have similar thermal conductivity values and density after drying. Meanwhile, formulation 54, which has lower thermal conductivity than the other three, also exhibits lower density after drying.

According to EN 998-1, mortars with thermal conductivity values below 0.1 W/m°C are classified as T1, and those between 0.1 and 0.2 are classified as T2. Mortars with thermal conductivity above 0.2 are not considered thermal mortars. As such, all the tested formulations could be classified as thermal insulation mortar. The thermal conductivity of the pastes decreases as the density decreases, with the incorporation of the damping materials (polyurethane and wood) proving to be very effective in further reducing this crucial parameter. The most performing formulation was classified as a 'T1 thermal mortar', and although the remaining pastes were classified as 'T2', their respective thermal coefficient was very close to the 'T1' threshold.

#### b) Thermal conductivity - Modified Transient Plane Source Method

Table 5 to presents the test results for the specimens in the dry state and also at a humidity level of 50% RH, 80 % RH and saturated. The value " $\lambda$ " represents the thermal conductivity value obtained from the modified transient plane source method test at an average temperature of approximately 30 °C, and " $\lambda_2$ " represents the same value after conversion according to ISO 10456 for an average temperature of 10 °C.

Table 5: Modified Transient Plane Source Method results at dry state.

Formulation	Average temperature (°C)	Specific Heat (J/kg°C)	$\lambda$ (W/m°C)	$\lambda_2$ (W/m°C)
42	31.0	553.35	0.101	0.107
45	30.9	924.71	0.102	0.109
47	30.5	1110.59	0.117	0.125
49	31.1	1597.91	0.159	0.169
54	31.1	1218.83	0.087	0.093

Table 6: Modified Transient Plane Source Method results at 50% RH.

Formulation	Average temperature (°C)	Specific Heat (J/kg°C)	$\lambda$ (W/m°C)	$\lambda_2$ (W/m°C)
42	31.9	568.78	0.104	0.111
45	31.5	1130.21	0.109	0.116
47	31.3	1160.06	0.127	0.136
49	31.6	1634.54	0.181	0.193
54	31.7	1286.77	0.093	0.099

Table 7: Modified Transient Plane Source Method results at 80% RH.

Formulation	Average temperature (°C)	Specific Heat (J/kg°C)	$\lambda$ (W/m°C)	$\lambda_2$ (W/m°C)
42	33.3	660.45	0.170	0.182
45	33.2	1385.84	0.138	0.148
47	32.9	1447.68	0.187	0.200
49	32.9	2319.18	0.299	0.320
54	34.0	1856.79	0.157	0.168

Table 8: Modified Transient Plane Source Method results at saturated state.

Formulation	Average temperature (°C)	Specific Heat (J/kg°C)	$\lambda$ (W/m°C)	$\lambda_2$ (W/m°C)
42	28.2	2234.05	0.744	0.786
45	26.9	2561.23	0.492	0.517
47	27.9	2717.69	0.530	0.559
49	27.8	2865.27	0.715	0.754
54	27.7	2521.73	0.446	0.470

As expected, the thermal conductivity values increase with the humidity level, as can be seen in Figure 13. It is also noted that the thermal conductivity at 50% RH, despite the slight increase, is very similar to the dry state.

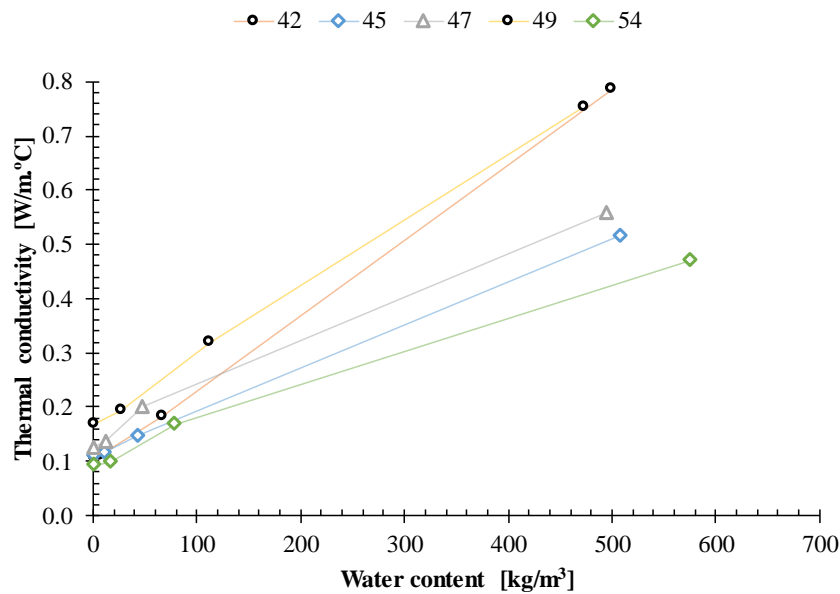


Figure 13: Thermal conductivity as a function of water content.

The formulations with the highest values at saturated state incorporate 3% polyurethane and 3% wood. Also, formulation 42 presented the highest variation, while the remaining formulations showed similar variation, comparing the dry with the saturated states.

#### c) Water content

Table 9 presents the five selected formulations' water content at different humidity levels.

Table 9: Water content at different humidity levels.

Formulation	Water content (kg/m³)		
	50 % RH	80 % RH	Saturated
42	6.79	65.79	499.93
45	11.08	43.36	508.58
47	12.16	47.82	495.15
49	26.31	112.06	473.38
54	16.19	78.42	575.05

It is possible to observe in Figure 14 the adsorption curves for the different formulations.

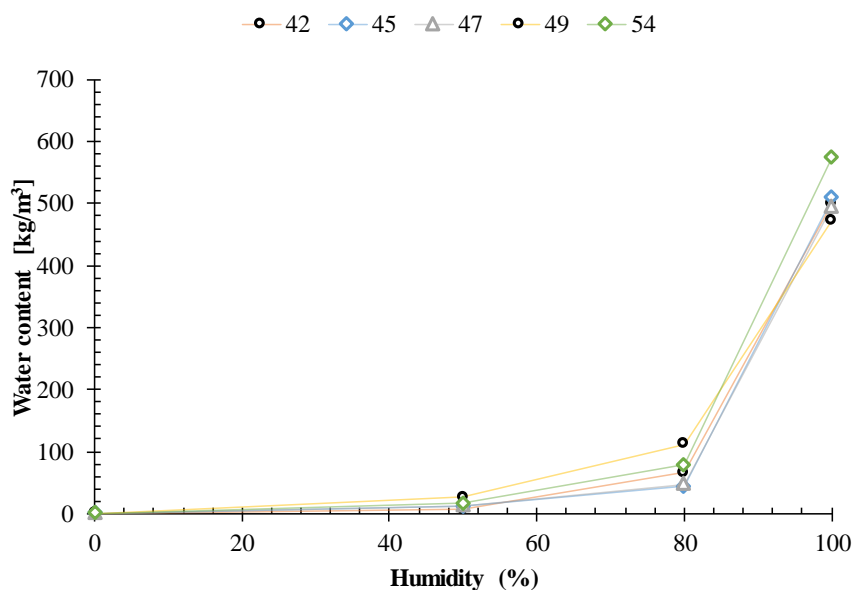


Figure 14: Water content at different humidity levels.

The obtained values are in the same order of magnitude. The lightest formulation (54) presented the highest water content value. Despite that, formulation 42 presented the highest variation in contrast with formulation 49, which showed the lowest variation.

#### d) Microstructural analysis

Based on the IUPAC classification, pores can be classified as micro ( $< 0.002 \mu\text{m}$ ), meso ( $0.002-0.05 \mu\text{m}$ ) and macro ( $> 0.05 \mu\text{m}$ ). Also, capillary porosity has a significant impact on the transportation process. Pores ranging from  $0.01$  to  $0.05 \mu\text{m}$  are classified as medium capillaries, while those ranging from  $0.05$  to  $10 \mu\text{m}$  are classified as large capillaries. Pores larger than  $10 \mu\text{m}$  are classified as air voids. By observing Figure 15, the MIP method allowed to identify a significant amount of mesopores and medium capillaries, evidencing a major porous structure with a relevant capillary net.



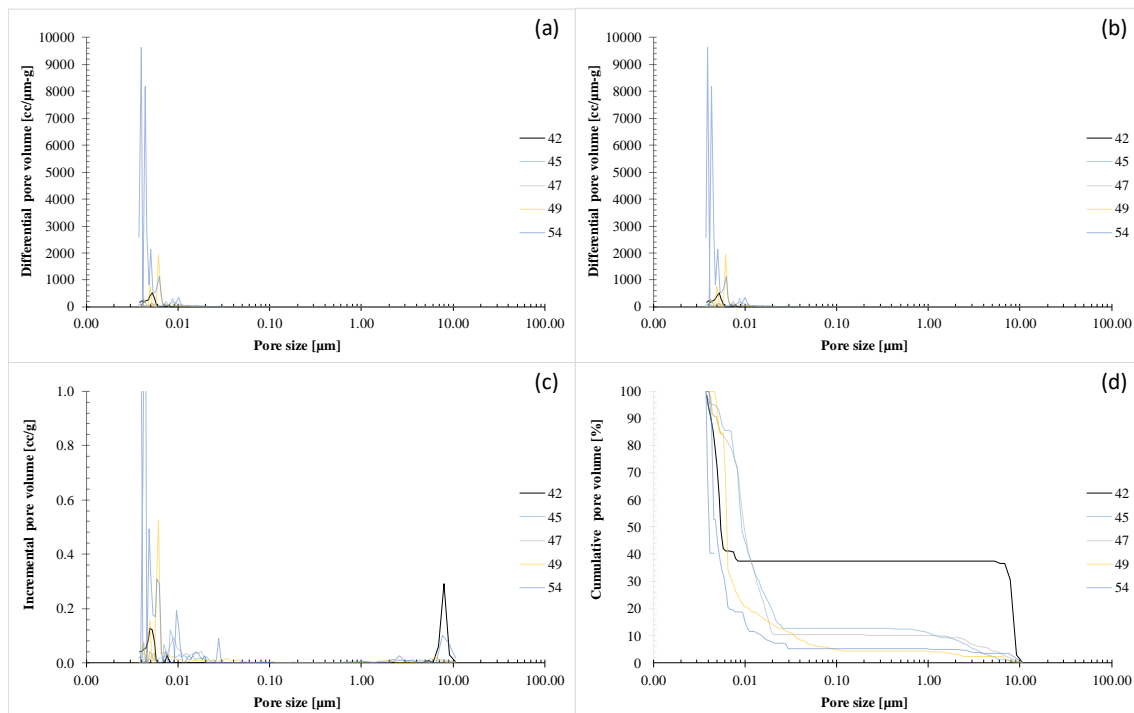


Figure 15: Porosimetry results.

Although the MIP technique is often employed to characterise pore structure, some degradation may occur due to the pressure exerted to inject the mercury. This degradation can be exacerbated by the lower mechanical strength of the tested material, which is the case with these lightweight pastes. Regarding porosity structure and volume, most pastes tested with MIP revealed mesopores and medium capillaries, suggesting a porous structure with a relevant capillary net.

Table 10 presents the bulk density and open porosity measured through hydrostatic weighing.

Table 10: Bulk density and open porosity.

Formulation	Bulk density (kg/m <sup>3</sup> )	Open porosity (%)
42	761.8	64.9
45	635.7	71.7
47	675.1	68.1
49	792.4	56.9
54	499.9	70.9

As can be seen in Figure 16, generally, the lower the open porosity the higher the density. Observing the different formulations, the distinct behaviour of formulations 45 and 54 are visible when replacing granite with marble, respectively. Even with the exact quantities of the various constituents, the incorporation of marble or granite leads to distinct densities for similar open porosity. The enclosed porosity present in polyurethane particles could be an explanation for these results.

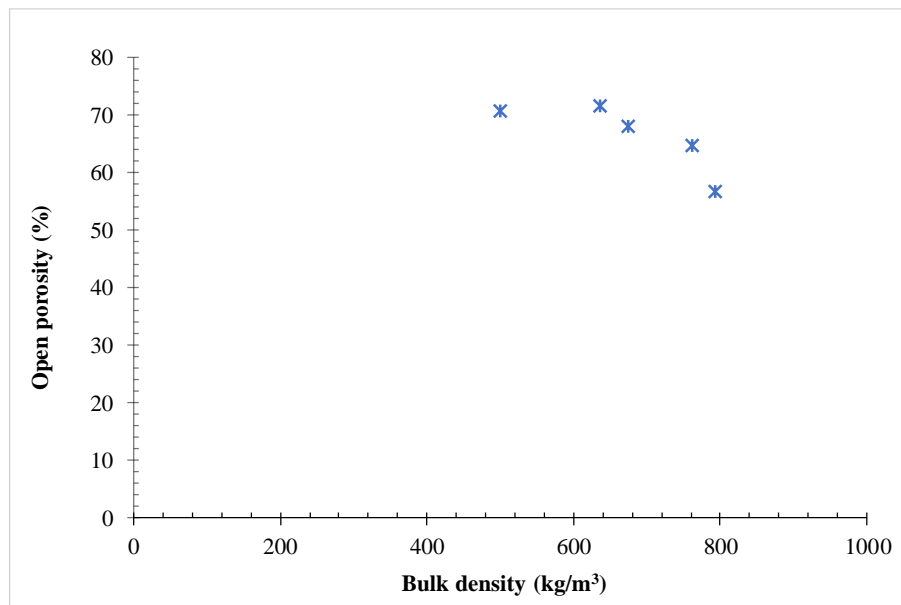


Figure 16: Open porosity as a function of bulk density.

g) Dynamic modulus of elasticity and Poisson's coefficient

Table 11 presents the dynamic modulus of elasticity and Poisson's coefficient.

Table 11: Dynamic modulus of elasticity and Poisson's coefficient.

Formulation	Dynamic modulus of elasticity (MPa)	Poisson's coefficient (-)
42	227	0.43
45	601	0.30
47	1058	0.24
49	326	0.36
54	461	0.34

The lower the dynamic modulus, the more elasticity and capacity of the material to absorb dimensional variations. However, a higher dynamic modulus implies improved mechanical resistance. As can be seen, formulation 47 presents a much higher value (approximately twice or more than the other formulations), which aligns with Poisson's coefficient results.

### 2.1.3. Formulations with nanoparticles

Table 12 shows the constitution of the selected formulations incorporating nanoparticles. The formulations with nanoparticles (indicated with an "n") were compared with the respective reference formulation (without nanoparticles).

Table 12: Selected formulations with nanoparticles incorporation for the hygrothermal characterisation

Formulation	Marble	Fly Ash	Slag	PU	Timber	Powdered Aluminum	S/L	H/S	Nanoparticle SiO <sub>2</sub> 60-70 nm
29	50%	50%	-	-	-	-	0.39	1.00	-
29n	50%	50%	-	-	-	-	0.39	1.00	0.5%
47	-	90%	-	5%	5%	0.1%	0.60	0.30	-
47n	-	90%	-	5%	5%	0.1%	0.60	0.30	0.5%
57	26	26	48	-	-	-	0.41	0.50	-
57n	26	26	48	-	-	-	0.41	0.50	0.5%

#### a) Thermal conductivity - Guarded Hot Plate Method

Table 4 shows the results obtained with the Guarded Hot Plate Method.

Table 13: Results of the Guarded Hot Plate Method

Formulation	Average temperature (°C)	$\lambda$ (W/m°C)	Classification EN 998-1
29	10.17	0.237	-
29n	9.89	0.238	-
47	9.85	0.103	T2
47n	9.94	0.113	T2
57	9.46	0.162	T2
57n	-	-	-

The incorporation of nanoparticles did not produce significant variation in the thermal conductivity, even when a slight increase was observed. Formulation 57, after being conditioned in the oven, became curved, which made it impossible to measure its thermal conductivity using the hot plate method. The specimens for this test need a smooth and flat surface to ensure the contact interface with the equipment remains intact.

Formulations 47, 47n and 57 could be classified as a T2 thermal mortar, according to EN 998-1 (thermal conductivity between 0.1 and 0.2 W/m°C). Formulations 29 and 29n are not considered thermal mortars, as already expected, regarding their high mass and dense microstructure.

b) Thermal conductivity - Modified Transient Plane Source Method

Table 5 presents the test results for the specimens in the dry state and also at a humidity level of 50% RH, 80 % RH and saturated. The value " $\lambda$ " represents the thermal conductivity obtained from the modified transient plane source method test at an average temperature of approximately 30 °C, and " $\lambda_2$ " means the same value after conversion according to ISO 10456 for an average temperature of 10 °C.

Table 14: Modified Transient Plane Source Method results at dry state (nanoparticle formulations).

Formulation	Average temperature (°C)	Specific Heat (J/kg°C)	$\lambda$ (W/m°C)	$\lambda_2$ (W/m°C)
29	31.7	1386.63	0.428	0.437
29n	30.3	1833.90	0.452	0.462
47	30.5	1110.59	0.118	0.125
47n	27.3	1114.75	0.114	0.120
57	28.3	840.83	0.151	0.160
57n	27.3	856.44	0.158	0.167

Table 15: Modified Transient Plane Source Method results at 50% RH (nanoparticle formulations).

Formulation	Average temperature (°C)	Specific Heat (J/kg°C)	$\lambda$ (W/m°C)	$\lambda_2$ (W/m°C)
29	29.8	1406.75	0.491	0.501
29n	30.4	1864.76	0.493	0.504
47	31.3	1160.06	0.127	0.136
47n	30.2	1266.81	0.128	0.136
57	30.8	1148.36	0.172	0.183
57n	31.3	1364.68	0.186	0.198

Table 16: Modified Transient Plane Source Method results at 80% RH (nanoparticle formulations).

Formulation	Average temperature (°C)	Specific Heat (J/kg°C)	$\lambda$ (W/m°C)	$\lambda_2$ (W/m°C)
29	30.8	1502.29	0.652	0.666
29n	31.6	1947.55	0.646	0.657
47	32.9	1447.68	0.187	0.200
47n	30.6	1480.81	0.194	0.206
57	32.4	1793.43	0.346	0.370
57n	32.7	1816.55	0.397	0.425

Table 17: Modified Transient Plane Source Method results at saturated state (nanoparticle formulations).

Formulation	Average temperature (°C)	Specific Heat (J/kg°C)	$\lambda$ (W/m°C)	$\lambda_2$ (W/m°C)
29	29.9	1751.33	1.086	1.107
29n	30.6	2208.85	1.088	1.111
47	27.9	2717.69	0.530	0.559
47n	31.5	2969.61	0.505	0.538
57	30.3	2268.89	0.693	0.736
57n	30.9	2244.08	0.694	0.739

As expected, the thermal conductivity values increase with the humidity level, but the incorporation of nanoparticles did not imply a distinct behaviour in the presence of water.

#### c) Water content

Table 18 presents the water content at different humidity levels for the selected formulations with nanoparticles.

Table 18: Water content at different humidity levels (nanoparticle formulations).

Formulation	Water content (kg/m³)		
	50 % RH	80 % RH	Saturated
29	17.87	57.99	132.02
29n	14.21	49.36	115.98
47	12.16	47.82	495.15
47n	9.35	51.68	379.57
57	3.76	67.39	198.48
57n	10.14	74.25	196.54

It is possible to observe in Figure 17 the adsorption curves for the different formulations. As can be seen, formulations 29 and 29n, as expected, presented a lower water content as they have a much denser structure. By contrast, formulations 47 and 47n presented higher values. Also, the incorporation of nanoparticles contributed to a reduction of the water content.

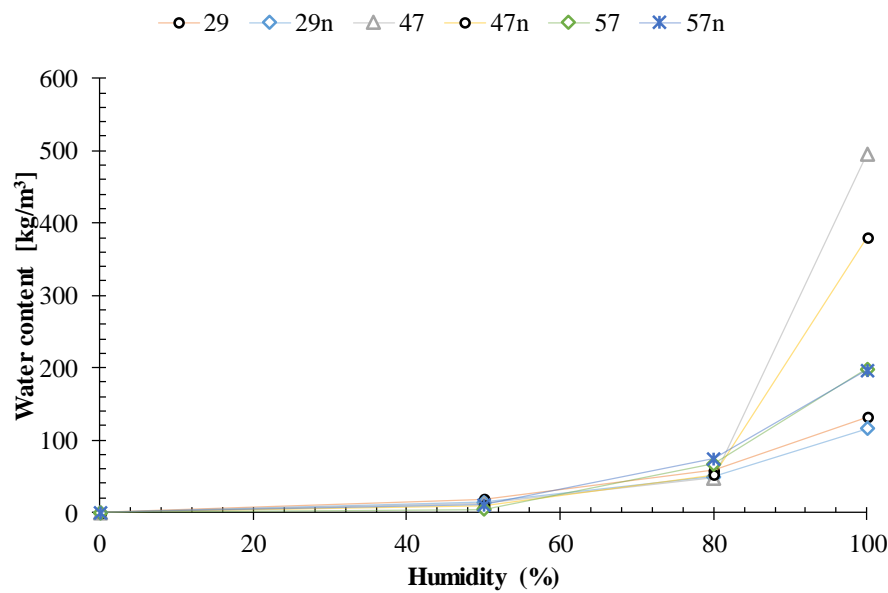


Figure 17: Water content at different humidity levels (nanoparticle formulations).

#### d) Microstructural analysis

By observing Figure 18, the MIP method allowed to identify a significant amount of mesopores and medium capillaries, evidencing a major porous structure with a relevant capillary net. As expected, formulations 29 and 29n revealed a completely different pore structure since they are much denser than the other samples, presenting a small number of pores. Regarding formulation 47, the incorporation of nanoparticles contributed to a reduction of pores diameter.



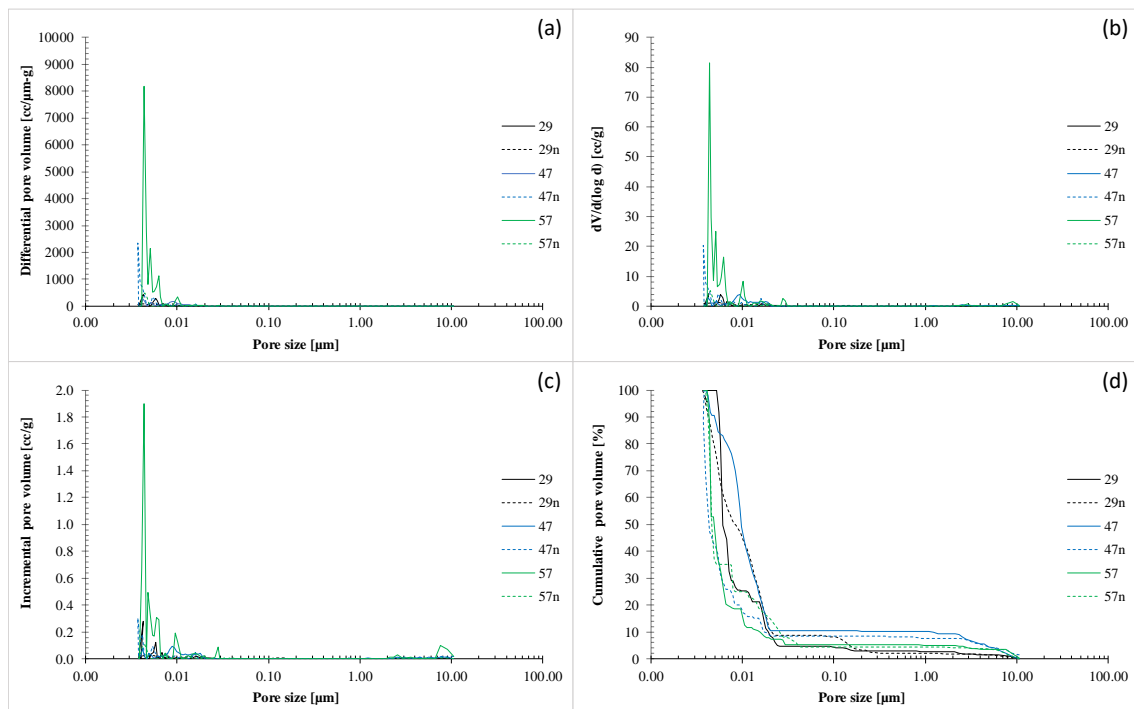


Figure 18: Porosimetry results (nanoparticle formulations).

Table 19 presents the bulk density and open porosity measured through hydrostatic weighing.

Table 19: Bulk density and open porosity (nanoparticle formulations).

Formulation	Bulk density (kg/m <sup>3</sup> )	Open porosity (%)
29	1474.5	36.8
29n	1461.6	36.2
47	675.1	68.1
47n	689.7	67.8
57	909.5	56.9
57n	950.7	54.5

The incorporation of the nanoparticles leads to a very slight reduction of the open porosity, which in the case of the lighter formulations (47, 47n, 57 and 57n) are in accordance with an increase of the bulk density.

#### h) Dynamic modulus of elasticity and Poisson's coefficient

Table 20 presents the dynamic modulus of elasticity and Poisson's coefficient.

Table 20: Dynamic modulus of elasticity and Poisson's coefficient (nanoparticle formulations).

Formulation	Dynamic modulus of elasticity (MPa)	Poisson's coefficient (-)
29	8849	0.28
29n	8814	0.28
47	1058	0.24
47n	891	0.29
57	1181	0.41
57n	1558	0.36

As expected, formulations 47 and 47n presented a lower dynamic modulus of elasticity. The incorporation of nanoparticles did not evidence a standard pattern.

## 2.2. Complementary characterisation of the final selected formulations

The formulation with a better compromise between the density, thermal and mechanical properties regarding the application purpose as a core insulation for SIP panels was the 47. As such, formulations 47 and 47n were deeply analysed regarding complementary hygrothermal and mechanical properties relevant to their intended application, as shown in Table 2.

Table 21 presents the complementary hygric properties measured for formulations 47 and 47n.

Table 21: Hygric properties

Hygric properties	47	47n
Water vapour permeability resistance factor – dry cup (-)	8.7	11.4
Water vapour permeability resistance factor – wet cup	6.1	8.3
Capillary water absorption – C (kg/m <sup>2</sup> .min <sup>0.5</sup> )	0.227	0.223

According to EN 998-1, the obtained results are admissible for thermal insulation mortars since the water vapour permeability resistance factor is lower than 15 and the capillary water absorption is below 0.4 kg/m<sup>2</sup>.min<sup>0.5</sup> (W1 classification).

Figure 19 shows a linear increase in the amount of absorbed water, allowing the classification as a Type A graph with no liquid water on the top surface, according to ISO 15148.

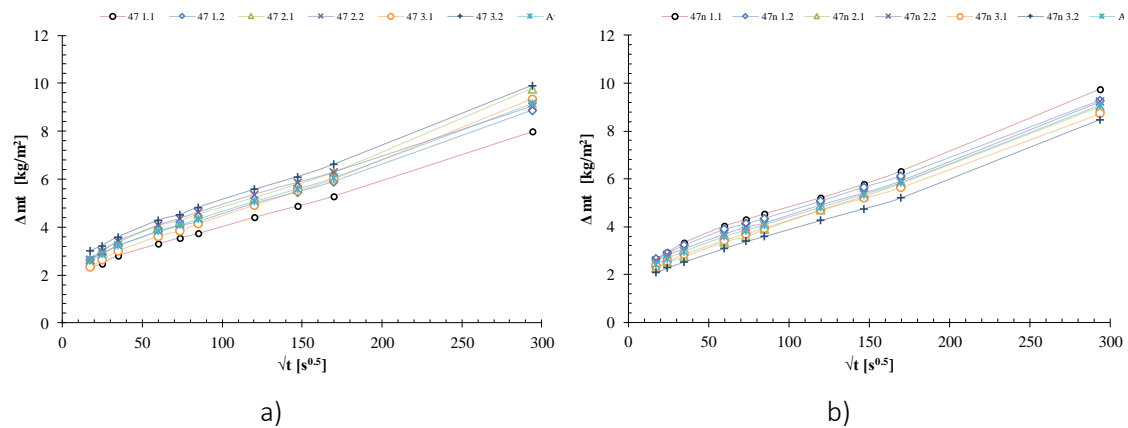


Figure 19: Capillary water absorption as a function of the square root of time for formulations (a) 47 and (b) 47n.

Table 22 presents the adhesive strength of the formulations to the OSB panel. This test was performed regarding the intended application of the formulations as core insulation of SIP panels. As such, two different approaches were tested:

1. Curing of the core formulation directly on the OSB board: application of a primer (in the case of its use) directly on the OSB board before placing the formulation paste (lines 1 and 2 of Table 22);
2. Curing of the core formulation separately, as a single board, and then glued to the OSB with polyurethane glue or an adhesive mortar, as shown in Figure 20 (lines 3 and 4 of Table 22).

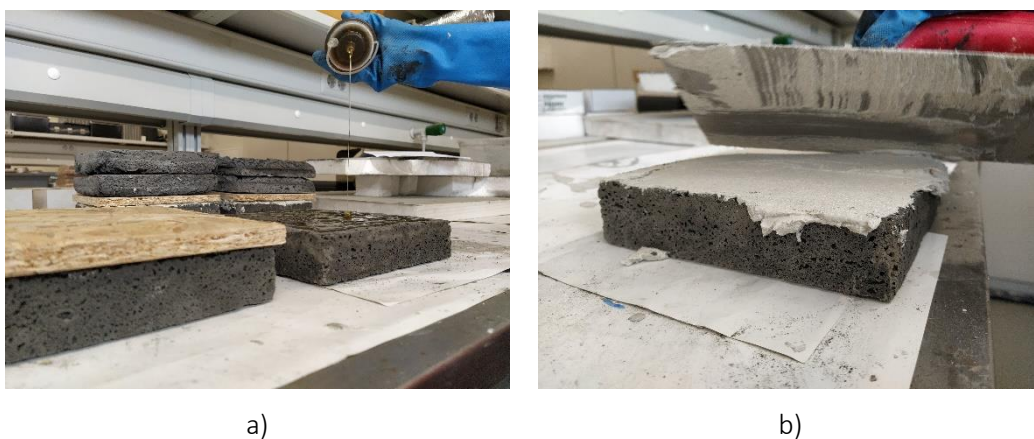






Figure 20: Application of (a) polyurethane glue and (b) adhesive mortar.


Table 22: Adhesive strength – Formulation 47 (F47).

Adhesive material	Adhesive strength (MPa)	Type of rupture	Visual observation
1. None	0.20	Predominantly adhesive ruptures (OSB-F47 interface)	
2. Universal primer	0.17	Cohesive ruptures (in the F47 itself)	
3. Polyurethane glue	0.31	Cohesive ruptures (in the F47 itself)	
4. Adhesive mortar	0.19	Predominantly adhesive ruptures (OSB-adhesive mortar interface)	

As can be seen, it is mandatory to use a product that improves the adherence between the core formulation and the OSB board, avoiding adhesive ruptures. Polyurethane glue, commonly used to glue the EPS slabs to the OSB boards to produce traditional SIP panels, showed the highest adhesive strength.

As such, formulation 47n was only tested using polyurethane glue, as shown in Table 23. The results are very similar to those obtained with formulation 47. However, not all the ruptures were cohesive as required.

Table 23: Adhesive strength – Formulation 47n (F47n).

Adhesive material	Adhesive strength (MPa)	Type of rupture	Visual observation
Polyurethane glue	0.30	Predominantly cohesive ruptures (in the F47n itself)	

Despite the low adherence values, these align with those verified in thermal mortars.

Considering the results of the complementary analysis, it was decided to produce the SIP panels using Formulation 47, considering the best compromise between the hygrothermal and mechanical properties.

### 2.3. Effect of different curing conditions

Also, the selected core insulation material was analysed in terms of the curing process – hot (drying in the oven) or ambient conditions – by a preliminary thermal conductivity and adhesion analysis. Figure 21 shows a specimen after curing in ambient conditions.



Figure 21: Formulation 47 after ambient curing on the top of the OSB board.

The visual aspect is similar to the samples cured in the oven. However, it is notable a more homogeneous structure but more brittle. One crucial aspect is the time needed to reach the hardened state, which is considerably higher using ambient conditions.

A thermal conductivity of  $0.09 \text{ W/m}^\circ\text{C}$  was obtained for the dry state using the Modified Transient Plane Source Method (see Figure 22). The result is lower than the samples cured in the oven, allowing classification as T1 thermal insulation mortar, which could be related to the different microstructure.





Figure 22: Thermal conductivity measurement of formulation 47 with ambient curing.

Table 24 presents the adhesive strength tested using the universal primer and polyurethane glue.



Table 24: Adhesive strength – Formulation 47 (F47) with ambient curing.

Adhesive material	Adhesive strength (MPa)	Type of rupture	Visual observation
2. Universal primer	0.08	Cohesive ruptures (but very close to the interface)	
3. Polyurethane glue	0.15	Cohesive ruptures (in the F47 itself)	

Despite the cohesive ruptures, the adhesive strength is considerably lower than the values obtained before with the oven curing. This is critical since the production process and the SIP panels require adequate mechanical resistance. As such, the core formulations for the SIP panels were produced considering oven curing conditions.

### 3. Hygrothermal characterisation of finishing render solutions

Two distinct finishing systems were defined as interesting solutions for using the new SIP panels (see Table 25):

- Rendering system applied on the sandwich panel for SIP construction: the rendering system consists of a new waste-based render and an acrylic paint incorporating SiO<sub>2</sub> nanoparticles);
- Ventilated façade: SIP sandwich (OSB panels and the core insulation material) plus a façade cladding made of the same material as the core. The façade cladding could also be painted with acrylic paint incorporating SiO<sub>2</sub> nanoparticles.

Table 25: Composition of the waste-based render and the ventilated façade panel.

System	Fly ash	Glass	CDW	Polyurethane	Timber	Powdered aluminium	S/L
Waste based render	25 %	25 %	50 %	-	-	-	0.32
Ventilated façade panel	90 %	-	-	5 %	5 %	0.1 %	0.60

The optical properties of the surface – reflectance, colour and emissivity – were deeply explored and presented in the A3 report at the time of the nanoparticles study and production of the panels for the durability assessment in SINTEF. As such, regarding the importance of the mechanical performance of such products, the adhesive strength and the hard body impact resistance were determined.





The adherence of the waste-based render was tested with the same methodology presented in 2.2 and shown in Figure 23 and Table 26.



Figure 23: Application of the (a) primer and (b) waste-based render on the OSB board.

Observing Table 26, the polyurethane glue presented the best adherence to the OSB panel again.

Table 26: Adhesive strength of the waste-based render.

Adhesive material	Adhesive strength (MPa)	Type of rupture	Visual observation
1. None	- (rupture at the time of the pre-cuts)	Adhesive ruptures (OSB interface)	
2. Universal primer	- (rupture at the time of the pre-cuts)	Adhesive ruptures (OSB interface)	
3. Polyurethane glue	0.31	Adhesive and cohesive ruptures (OSB interface)	
4. Adhesive mortar	0.19	Adhesive ruptures	

The hard body impact resistance was determined for the two systems under study based on EN 13497 using the Martinet Baronnies apparatus, considering 3 J impact energy, as shown in Figure 24.

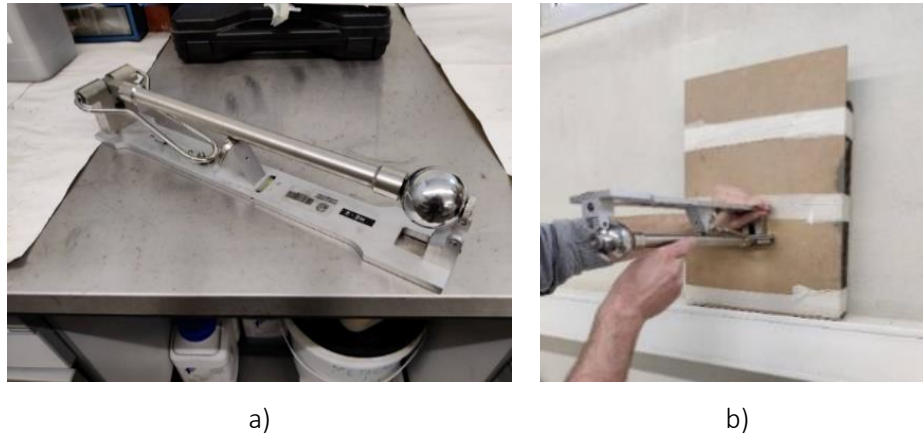


Figure 24: Hard body impact test: (a) Martinet Baronnies apparatus and (b) Preparation of the test set-up.

During the first impact, the waste-based render was completely broken, as can be seen in Figure 25-a). Three impacts were performed on the cladding panel with an average dent diameter of 14.2 mm (see Figure 25-b).



Figure 25: Hard body impact test results: (a) Waste-based render and (b) Cladding panel.

Regarding the results, the waste-based render is unsuitable for a rendering system application. In contrast, the cladding panel did not present any cracking or visible damage after impact.



#### 4. Hygrothermal characterisation of the SIP panel rendering system

The production of the prototypes (SIP panels) was one of the fundamental actions of the whole project since it is linked to the main objective. This step required the adaption and optimisation of the production process. Dreamdomus assembled and prepared all the panels needed for the testing.

This action was done in parallel with the Durability Assessment action of activity A3 concerning the production of the SIP panels (40x40x15 cm). As such, two stages were considered:

1. Small-scale SIP panels (40 x40 x15 cm) production for the durability assessment (Activity A3);
2. Real-scale prototype (200x200x15 cm) for testing the assembly and thermal performance (thermal resistance measurement).

The production method, prepared and tested by Dreamdomus, allowed a fast and easy assembling of the SIP panels, which was ultimately tested on constructing the SIP panel prototype wall.

UTAD prepared all the specimens required for both stages' core and rendering system. The core panels' execution, due to their dimension, requires extensive work for the preparation of constituents and treatment of wastes—also, the cleaning, assembling and conditioning of the moulds.

FEUP performed all the quantitative analysis of stage 1 and all the tests regarding stage 2, being the real-scale prototype installed at FEUP facilities.

Following the results presented in Chapter 3, a commercial base coat was applied, widely used by the construction industry.

##### 4.1. Small-scale SIP panels

The production of the panels, as well as the ageing procedure and qualitative analysis performed by SINTEF, were already described in the A3 Report.

FEUP developed the quantitative analysis, presented in the following topics.

#### 4.1.1. Optical properties

Figure 26 presents the average values and the standard deviation of emissivity and total reflectance of the three configurations before and after the accelerated ageing exposure.

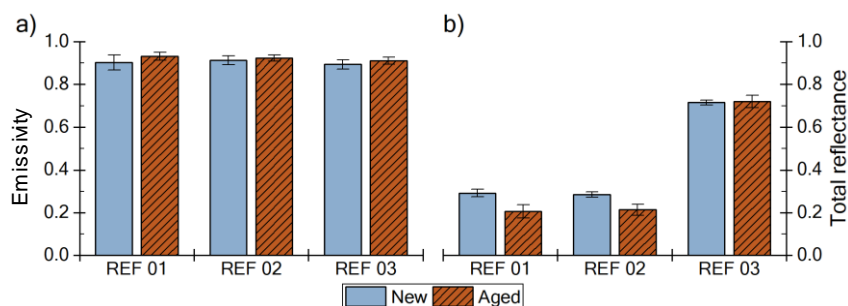


Figure 26: Initial and aged optical evaluation. a) Emissivity; b) Total reflectance.

The initial emissivity (Figure 26-a) ranges between 0.89 and 0.91, increasing to 0.91-0.93 after ageing (orange bar), which is non-significant. Also, the values align with coatings and renders commonly applied in façades. The total reflectance (Figure 26-b) reveals the finishing layer's aesthetic, where dark colours present a total reflectance lower than 0.4 and white/light colours higher than 0.7. The ageing effect on REF 03 is also insignificant, while on dark colours, REF 01 and REF 02, the reflectance reduces by more than 25%. The degradation stimulated by the accelerated process (NORDTEST) preconises the natural degradation. In these terms, the founded results are similar to those in the bibliography, where climatic agents unaffected emissivity values, e.g. temperature, humidity, or ice.

Observing Figure 27 and Figure 28, it is evident the ageing effect on the reduction of the solar reflectance of the dark coatings and also the impact of nanoparticle incorporation by the increase of the NIR reflectance. As expected, REF 03 (white primer) presented a completely different behaviour.



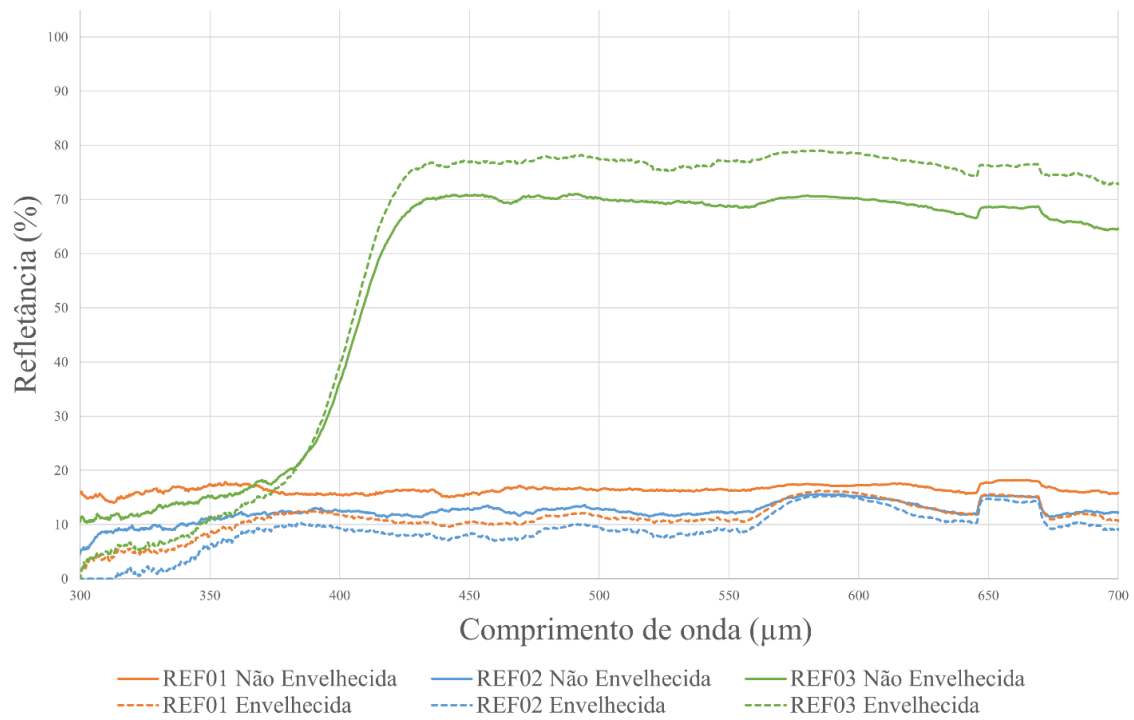


Figure 27: Reflectance in the UV-Vis region

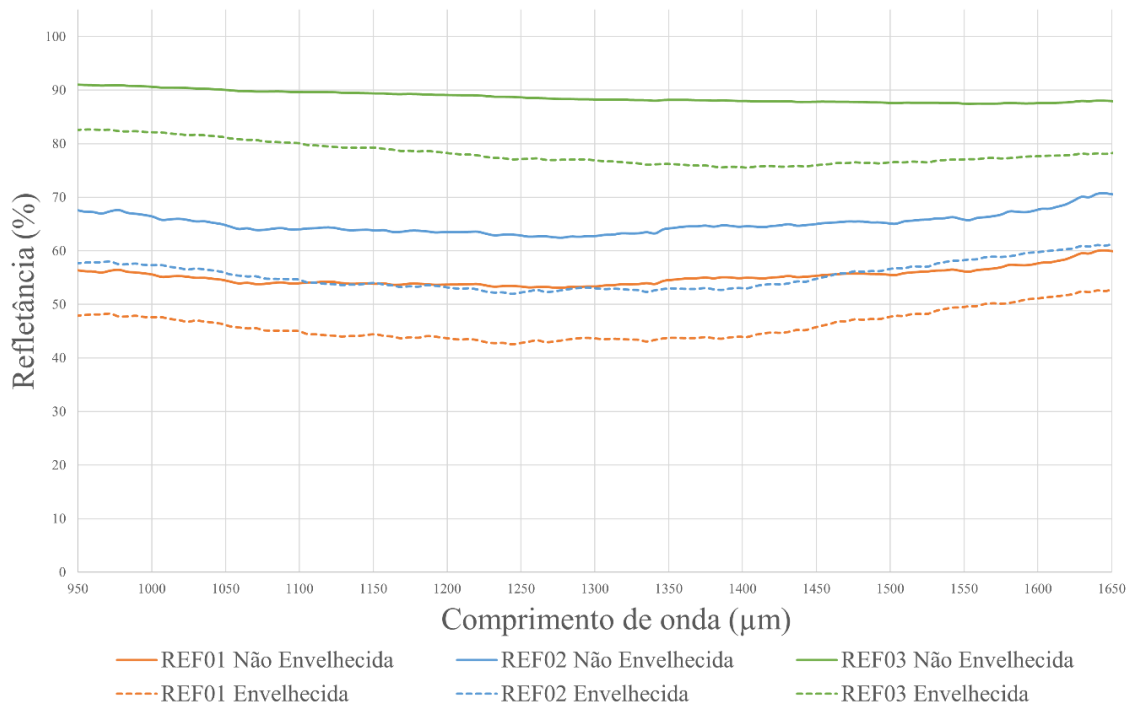


Figure 28: Reflectance in the NIR region.

Aesthetical properties, like colour, can be related to coatings' reflectance and thermal performance. Table 27 details the colour CIELab coordinates and the total colour difference for the samples after accelerated ageing.

Table 27: Colour coordinates and total colour difference.

SAMPLE	CONDITION	L	a	b	COLOUR DIFFERENCE
REF 01	New	47.95 ± 1.056	0.73 ± 0.560	1.26 ± 0.987	-
	Aged	46.94 ± 1.753	0.72 ± 1.405	3.35 ± 1.241	2
REF 02	New	44.08 ± 1.983	2.71 ± 0.940	1.13 ± 1.650	-
	Aged	45.97 ± 1.647	1.66 ± 1.565	3.82 ± 1.132	3
REF 03	New	86.88 ± 0.286	-0.65 ± 0.250	0.42 ± 0.360	-
	Aged	88.48 ± 1.034	-0.83 ± 0.558	1.89 ± 0.686	2

The lightness of nanoparticle samples is lower than the reference coating, respectively REF 02 and REF 01. The total colour difference indicates the colour perception imposed by the degradation, which, in this study, does not produce a significant modification to be perceptible for the human eye (higher than 3). The opposite effect is highlighted on lightness (L) since it was expected that the dark sample (REF 01 and REF 02) would become lighter and the white one (REF 03) darker (lower lightness). However, the observed increase is little.

#### 4.1.2. Hygric properties

The L-shape Karsten tube method measured the liquid water permeability according to RILEM Test Method - Test No. 11.4. All tests comprised three measurements in each specimen, adhering to the tubes as shown in Figure 29-a).

Regarding liquid water permeability, measured through the Karsten tube method, all the configurations did not absorb water under low pressure (volume of absorbed water = 0 ml). The ageing process did not affect the coatings when the acrylic paint was applied (REF 01 and REF 02) since no water was absorbed too. However, REF 03 registered a total volume of 0.07 ml at the end of the test (60 minutes). This was expected regarding the characteristics of the universal primer and the microcracks observed in REF 03 (see Figure 29-b).

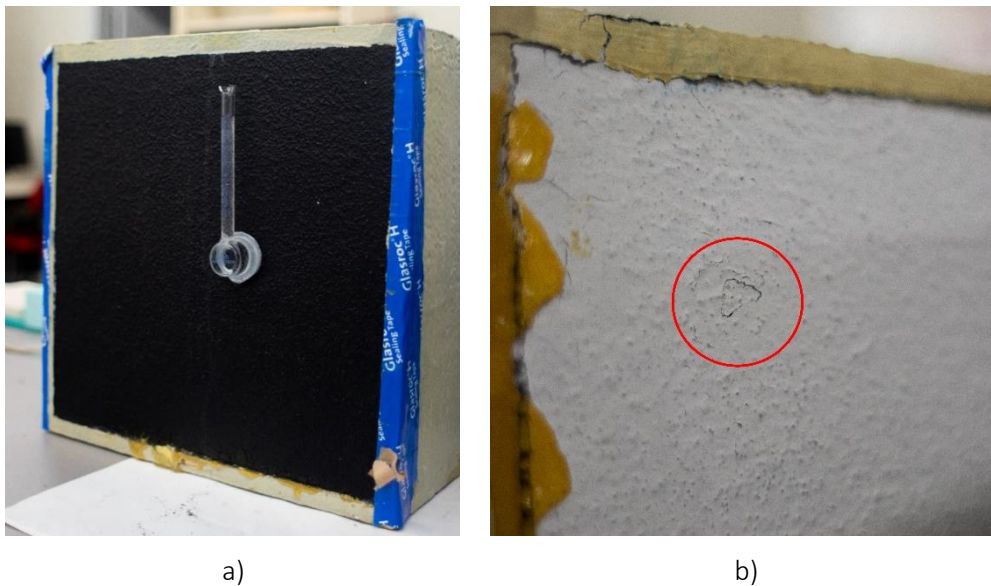





Figure 29: (a) Liquid water permeability test and (b) Cracking in REF 03 after ageing.

#### 4.1.3. Mechanical properties

##### a) Adhesive strength

Table 28 presents the adhesive strength of the small-scale SIP panels before ageing. As can be seen, all the ruptures were adhesive between the OSB and base coat, with very low adhesive strength.

Table 28: Adhesive strength before ageing – small-scale SIP panels.

Reference	Adhesive strength (MPa)	Type of rupture	Visual observation
REF 01	0.17	Adhesive ruptures (OSB-base coat interface)	
REF 02	0.19	Adhesive ruptures (OSB-base coat interface)	
REF 03	0.14	Adhesive ruptures (OSB-base coat interface)	

After ageing, the ruptures occurred during pre-cutting, invalidating the adhesive strength measurement. All the ruptures were again adhesive.

#### b) Hard body impact resistance

The hard body impact resistance was determined using the Martine Baronnée apparatus, as shown in Figure 30.

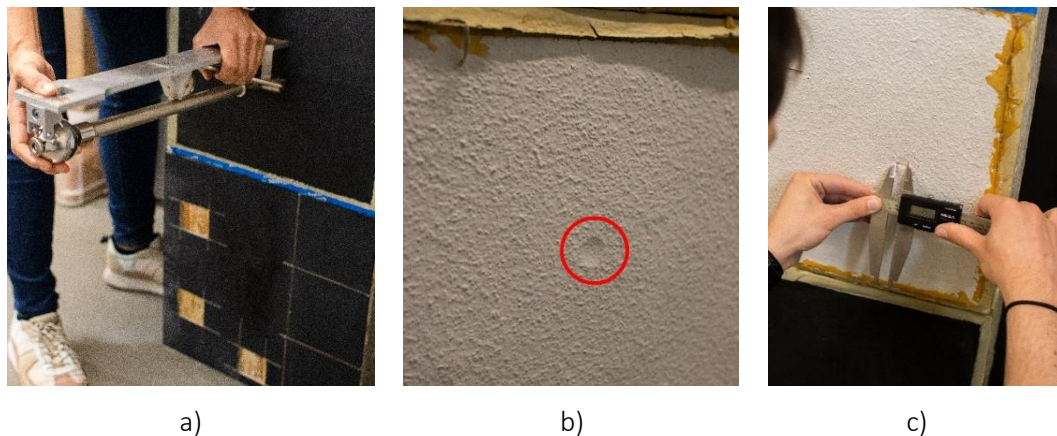


Figure 30: a) Hard body impact test; b) Example of dent identification; c) Dent diameter measurement.

The results are presented in Table 29, and it is possible to observe a slight increase in the dent diameter after ageing. However, any cracks or delamination were visible after the apparatus's impact.

Table 29: Hard body impact results – small-scale SIP panels.

Reference	Average dent diameter (mm)		Visual observation
	Before ageing	After ageing	
REF 01	11.6	14.3	Without cracking or delamination
REF 02	12.1	13.2	
REF 03	13.0	13.8	

## 4.2. Real-scale prototype

### 4.2.1. Prototype installation

The real-scale prototype consists of a SIP wall of 2x2 m<sup>2</sup> which was coupled to a climatic chamber to measure the thermal resistance. The interior part of the chamber simulated a cold climate (low temperatures), creating a heat flux with the outside surface that is in contact with the laboratory ambient conditions. As such, the panels have the same configuration tested before. The exterior surface (facing the interior of the chamber) was prepared by combining the three previous references tested in 4.1 (see Figure 31-a).

The previous results were all considered for the real-scale prototype's development. For example, the observed adhesive ruptures led to the application of an additional layer (rough adherence primer, as shown in Figure 31-b) between the OSB board and the base coat to improve adherence.

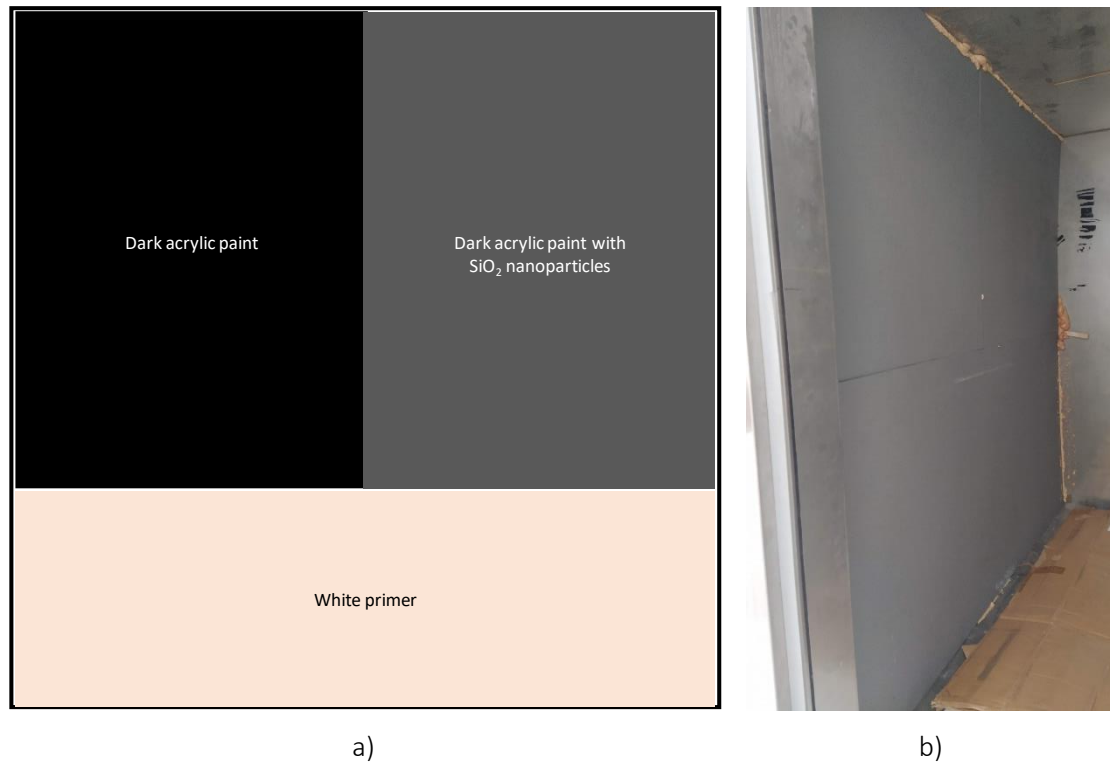


Figure 31: a) Surface layout of the real-scale prototype; b) Rough adherence primer.

Since the production of the panels was already tested and the assembly as a prefabricated component in 4.1, traditional assembly was also evaluated to cover a wide range of methods. This also allowed to test the use of the core panels without surface treatment (cutting to achieve flatness) by using polyurethane foam (see Figure 32).





Figure 32: Core panels assembled.

After placing the OSB panel with the rough adherence primer, the rendering system was applied: two layers of a commercial base coat reinforced with a glass fibre mesh (see Figure 33) and the finishing coatings (white primer and black acrylic paint with and without nanoparticles (see Figure 34).



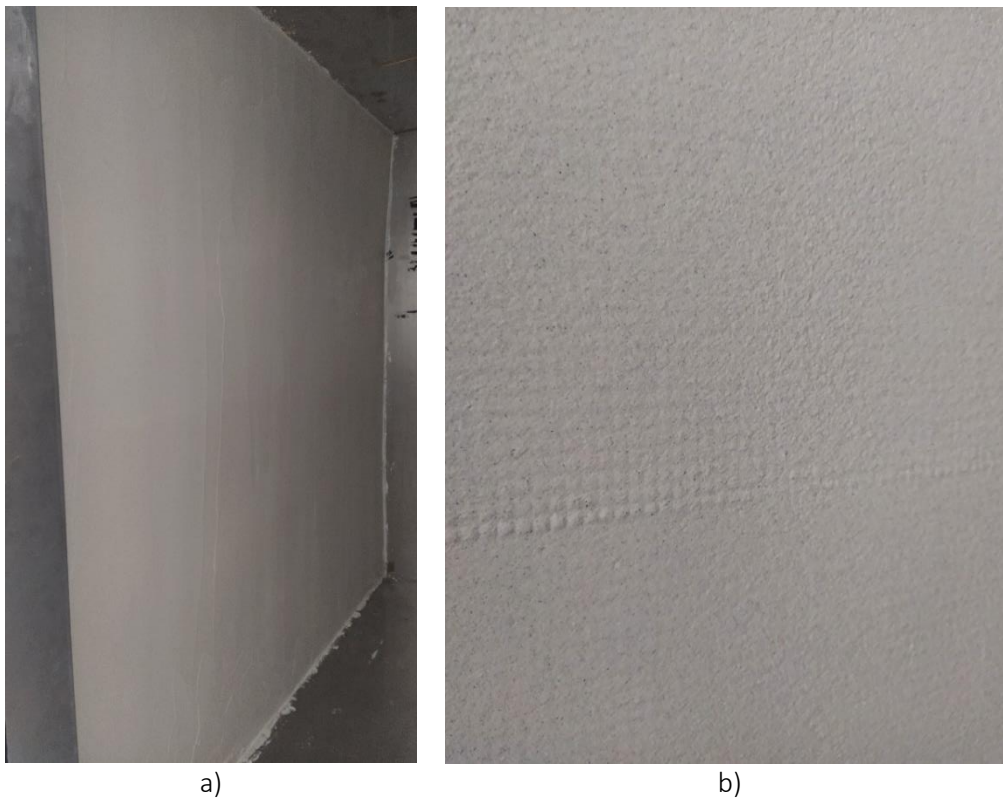


Figure 33: Application of the rendering system: a) Base coat; b) Glass fibre mesh embedded into the base coat.

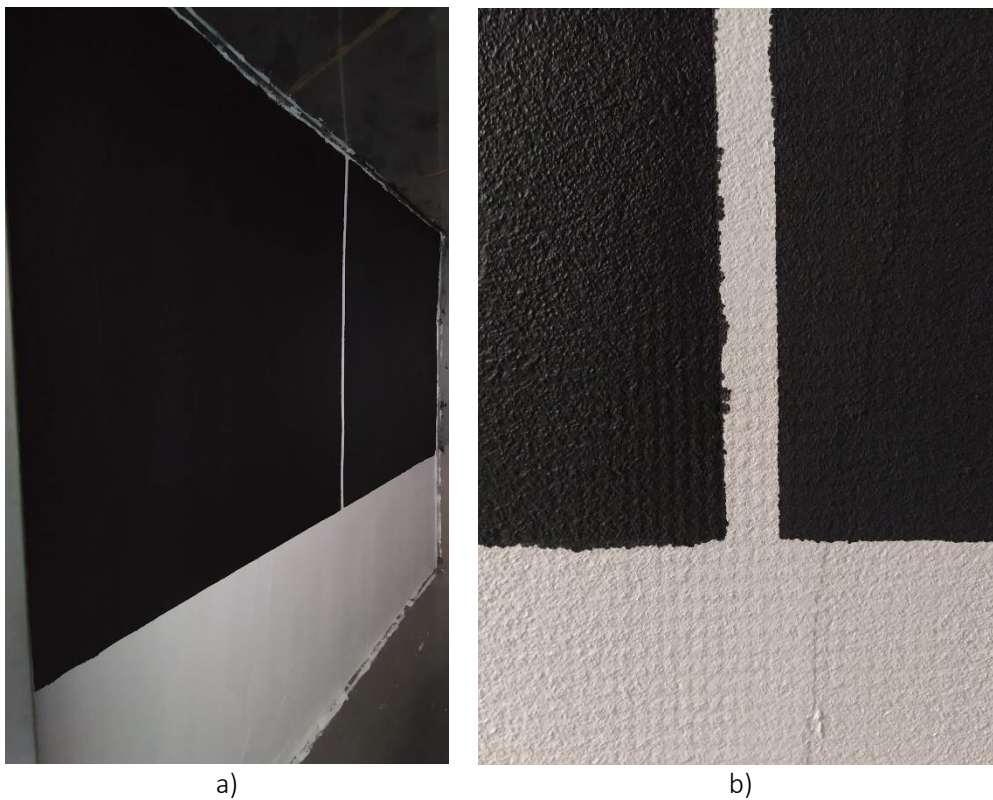


Figure 34: Application of the finishing coating system: a) Overview; b) Detail.

#### 4.2.2. Thermal resistance measurement

The thermal resistance was measured using flux meters and surface temperature sensors in two distinct zones: the middle of the core panel and the joints between panels, as shown in Figure 35.

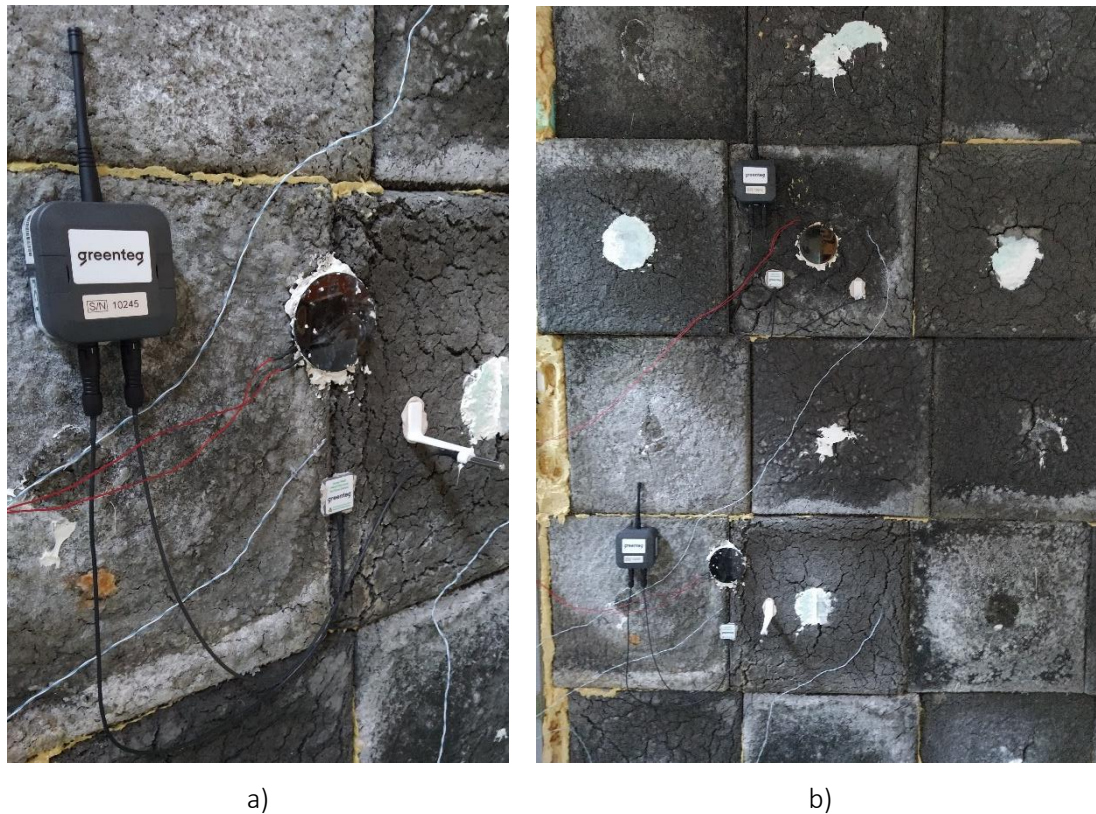


Figure 35: a) Equipment for the thermal resistance measurement; b) Placement in the different zones of measurement.

The results showed a thermal resistance of  $1.1 \text{ W/m}^2.\text{K}$

#### 4.2.3. Experimental assessment

After the prototype was subject to temperature and relative humidity variation, a qualitative analysis allowed to observe the visual aspect of the surface. As can be seen in Figure 36, no damages were observed. It should be highlighted that the exposition conditions were moderate.

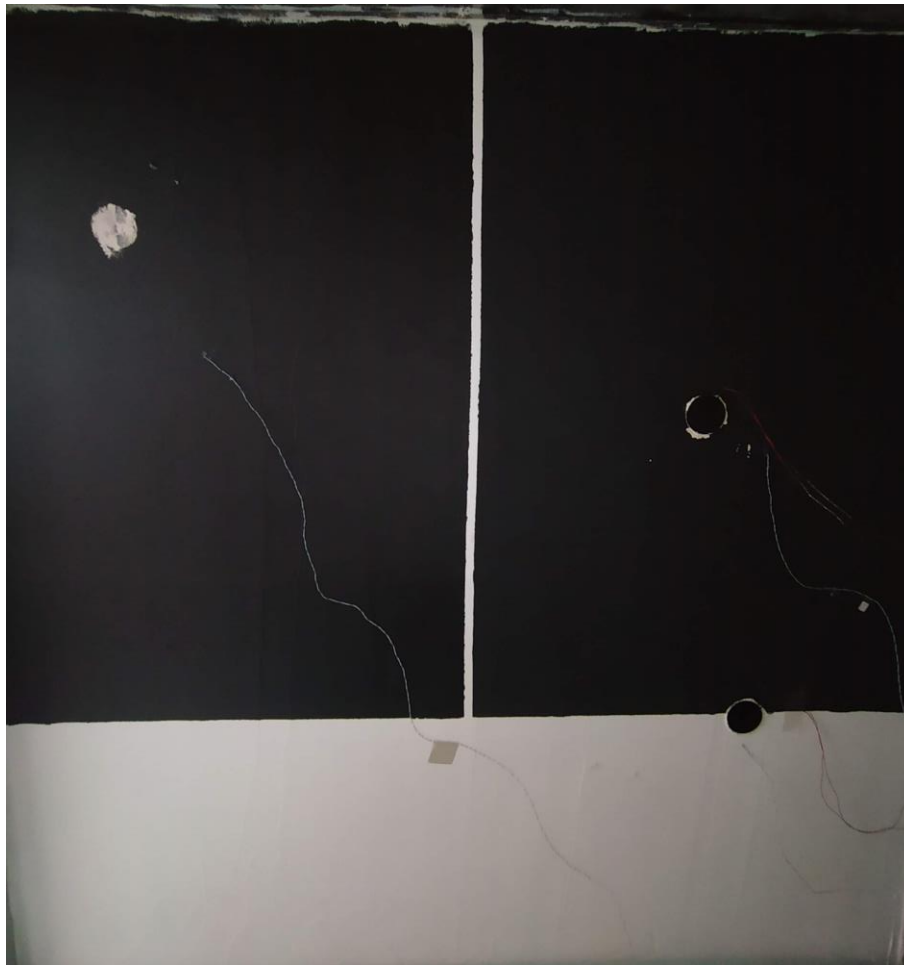


Figure 36: Visual aspect after exposition to cold temperatures.

c) Hard body impact resistance

Figure 37 presents the hard body impact resistance determined using the Martine Baronnie apparatus, regarding the mechanical analysis.



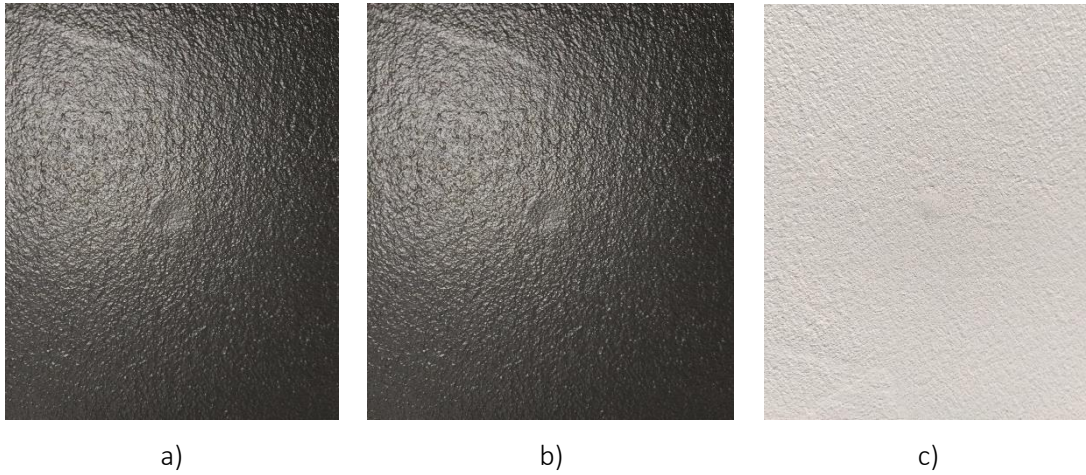


Figure 37: Hard body impact test: a) REF01, b) REF02 and c) REF03.

The results are presented in Table 30, and it is possible to observe

Table 30: Hard body impact results – real-scale prototype.

Reference	Average dent diameter (mm)	Visual observation
REF 01 (black paint)	10.1	Without cracking or delamination
REF 02 (black paint with nanoparticles)	11.2	
REF 03 (white primer)	10.5	